Proceedings of the ASME 2023
Verification, Validation, and Uncertainty Quantification Symposium
VVUQ2023
May 17-19, 2023, Baltimore, Maryland

VVUQ2023-107659

Digital Image Correlation Validation of Finite Element Strain Analysis of Dental Implant Insertion for Two Implant Designs

Baixuan Yang
Queen's University
Kingston, Canada

Ainara Irastorza-Landa
Nobel Biocare Services AG
Kloten, Switzerland

Peter Heuberger
Nobel Biocare Services AG
Kloten, Switzerland

Heidi-Lynn Ploeg
Queen's University
Kingston, Canada

ABSTRACT

Sufficient anchorage of dental implants, defined as mechanical engagement between implant and bone at the time of insertion, has been recommended for positive clinical outcomes, particularly in immediate loading protocols. Accurate measuring and analysis of stress and strain in the bone are imperative to understand anchorage from the biomechanics perspective. However, the stress and strain distributions at the bone-implant interface are impossible to measure *in vivo*. Therefore, the aim of this study was to develop and validate an explicit continuum finite element analysis (FEA) to investigate the stress and strain in a bone surrogate during the insertion of a dental implant: with cutting flute (CF) and without (NCF). Ten dental implants (five with CF and five with NCF) were inserted into ten rigid polyurethane (PU) foam blocks with a prepared pilot hole. During the insertion, a stereo digital image correlation (DIC) system was used to record in-plane deformation on the PU foam surface at a frequency of 1.0 Hz; and, surface *von Mises* strain,ε_{v_DIC}, was calculated (VIC-3D, Correlated Solutions Inc). In parallel, the insertion was simulated using FEA with explicit solver (Abaqus Explicit version 2017, Simulia). The PU foam was defined as an elastic-plastic material with a progressive crushable foam failure behaviour. The surface *von Mises* strain predicted from FEA, ε_{v_FEA}, was compared against ε_{v_DIC}. Uncertainty of DIC displacement measurement was 0.6 µm; and the static noise floor for the strain measurement was 500 microstrain ($\mu\varepsilon$). Coefficient of determination for ε_{v_DIC} and ε_{v_FEA} along a horizontal line for the CF and NCF implants were 0.80 and 0.78, respectively, which suggested the overall FEA performance was good. FEA results indicated that the cutting flute reduced the maximum shear stress in the PU foam and axial force which facilitated the insertion with less effort. This study demonstrated the successful combination of mechanical testing and FEA to better understand the mechanics of dental implant insertion.

Keywords: Dental Implant, FEA, DIC, Insertion

NOMENCLATURE

ε_{v_DIC}	*von Mises* strain measured by digital image correlation
ε_{v_FEA}	*von Mises* strain predicted by finite element analysis
ε_{x_DIC}	In-plane strain in x-direction measured by digital image correlation
ε_{y_DIC}	In-plane strain in y-direction measured by digital image correlation
u	Displacement in x direction, mm
v	Displacement in y direction, mm
ε_v	*Von Mises* strain
ε_1	Maximum principal strain
ε_2	Minimum principal strain
E	Apparent elastic modulus, MPa
ε	Engineering strain
E^L	Elastic moduli of loading path, MPa
E^U	Elastic moduli of unloading path, MPa
ε^{pl}	Equivalent plastic strain
$\dot{\varepsilon}$	Strain rate
η	Stress triaxiality
D	Overall damage variable
E_0	Initial apparent elastic modulus, MPa
ε_p	Average plastic strain
ε_{v_max}	Maximum *von Mises* strain over the entire region of interest at the final insertion depth (11.5 mm)

1. INTRODUCTION

Dental implants are considered a favourable treatment option for the rehabilitation of missing teeth, anchoring into the surrounding bone and supporting dental prostheses [1]. From the biomechanics perspective, they are designed to promote good

bone-implant mechanical engagement. This fixation at the time of insertion is defined as anchorage. Sufficient anchorage of the implants is one of the requirements for osseointegration, "a direct structural and functional connection between ordered, living bone, and the surface of a load carrying implant", which has been recommended for positive long-term clinical outcomes, especially for immediate loading of implants [2]. Therefore, it is important to analyse and measure the stress and strain distributions in the bone during implant insertion to comprehensively understand the bone-implant mechanical engagement.

In the dental biomechanics research, various transducers have been used to measure deformation and strain such as strain gauges, linear variable differential transformers (LVDT) and deflectometers [3,4]. These conventional methods are sensitive to the environment and difficult to implement. They require transducer contact with the sample, which is difficult in small implants and makes it impossible to provide full-field strain measurement [4].

To overcome the limitations of conventional techniques, digital image correlation (DIC) deformation measurement has been introduced in this field recently [5]. The DIC is capable of providing a full field deformation and strain measurement without contact by comparing grayscale images before and after deformation [6]. This method is simple and easy to implement regardless of the specimen type and size and without disturbing the specimen. Therefore, it has been attractive for dental research [7]. Initially, it was applied to measure the mechanical properties of dental implant material [7], and polymerization shrinkage behaviour of dental resin composites [8]. Tiossi et al. conducted a series of studies with stereo-DIC to investigate the bone surrogate surface strain distribution surrounding implant-supported prostheses with different splinting designs and crown material [9,10]. Later, they used validated Finite Element Analysis (FEA) to predict strain induced from the implant-support prostheses. The FEA was validated by comparing the predicted bone surrogate surface strain with DIC measurements [11]. Clelland et al. measured strain distribution on the bone surrogate surface, generated by applying 400 N load in the vertical and oblique directions on cement-retained implant crowns using stereo-DIC [12]. Many studies have shown that stereo-DIC is successful to investigate the strain transfer behaviour of different implant abutment designs [13,14]. However, little research has been conducted to measure with DIC the strain on the bone surrogate surface during the insertion of dental implants.

Computational models such as FEA are a powerful tool to predict stress and strain, especially in locations where it is impossible to measure directly [15]. However, the credibility of the FEA must be established to validate the accuracy of the model predictions for its intended use. The model credibility is generated with verification and validation (V&V) processes [16]. More specifically, verification determines if the model is implemented correctly while the validation assesses the error and uncertainty in the model predictions according to American Society of Mechanical Engineers Committee [17]. To assess accuracy, data from well-defined validation experiments are directly compared to the FEA results. However, validation experiments are difficult to conduct; therefore, sometimes published validation data or analytical models are used for validation. A recently published review argued that FEA with sufficient validation is still rare in dental biomechanics. Only 47 papers met the validation criteria out of 522 published articles from 1997 to 2016 [15]. In addition, nine of the 47 were compared against data in literature and two of them were compared against FEA results from analyses performed in other FEA software applications. The ideal validation process should be conducted in a hierarchical fashion: unit problem; benchmark against a known solution; the subsystem; and, finally the complete system [17,18].

FEA of dental implant insertion is challenging due to the complex, large deformation bone-implant contact, and non-linear material properties including damage accumulation. Van Staden et al. and Guan et al. generated FE models to predict stress distribution in jawbone during insertion. Both FEAs applied an insertion torque on the implant to predict jawbone deformation with nonlinear material models [19,20]. However, a limitation of these FEAs was that they did not include bone damage, which is known to greatly impact the ability of the bone to carry load [21]. Dorogoy et al. improved FEA with a damage criterion and element deletion; however, the FEA results were not compared with experimental data [22]. The latest study published by Ovesy et al. performed a micro-FEA (μ-FEA) to predict the insertion torque (IT) of a dental implant into bovine tibias with experimental IT data for validation. However, they stated that the μ-FEA was more time consuming compared to Dorogoy et al.'s work [21]. There is lack of continuum FEA studies on dental implant insertion with validation against experiments or analytical models [23].

The aim of this study was to develop and validate an explicit continuum FEA to investigate the strain on the bone surrogate surface during the insertion of a dental implant with and without a cutting flute. The insertion process was physically conducted and simulated in parallel; and, the bone surrogate surface strain was measured using stereo-DIC for FEA validation.

2. MATERIALS AND METHODS

2.1 Dental Implant Insertion Testing with Digital Image Correlation

The commercially available implant (NobelActive® NP 3.5 x 13 mm, Nobel Biocare AB, Göteborg, Sweden), 3.5 mm in diameter, total length of 12.5mm and a body thread length of 11.5 mm, was modified for this study: with cutting flute (CF) and without CF (NCF), to investigate effect of the cutting flute in the apex shown in Fig.1. The implants were inserted into rigid polyurethane (PU) foam blocks (0.32 g/cm^3, 20 PCF, SKU 1522-03, Sawbones®, Pacific Research Laboratories Inc, WA, USA) with a final insertion depth of 11.5 mm, leaving the collar of the implant above the bone level by 1 mm. All PU foam (40 × 40 × 8 mm) and stepped pilot holes (2.4/2.8 mm in diameter and 12.5 mm in depth; Article No.32261, Nobel Biocare AB,

Göteborg, Sweden) were prepared using a mill machine. The insertion tests with five repeats (five implants each with CF and NCF) were conducted under constant angular and axial velocity control (7.5 rpm and 0.3 mm/s, respectively) using an Electroforce 3230-AT Series III (TA instruments, ElectroForce Systems Group, Eden Prairie, Minnesota, USA) at room temperature in dry conditions, shown in Fig.1.

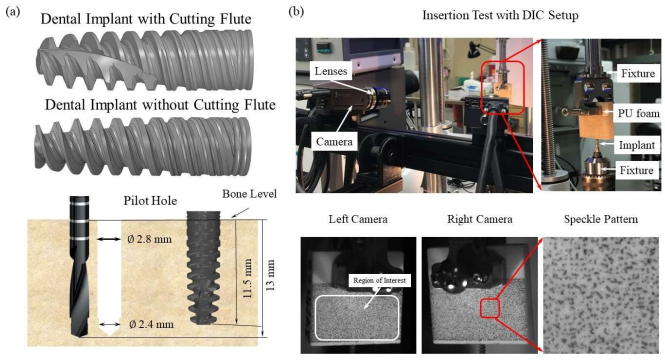

Figure 1: (a) ∅ 2.4/2.8 mm stepped pilot hole and insertion depth. (b) Top: Insertion testing with stereo-DIC setup. Bottom: an example of the image and the speckle pattern.

Stereo DIC was used to measure deformation on the surface of the PU foam during the test. The front surface of the foam was painted using an ink stamp with a random black speckle pattern which was generated using a commercial speckle pattern generator software with 50 % density and 50% variation (Correlation Solutions Inc, Irmo, South Carolina), shown in Fig.1b. Images were captured at a frequency of 1 Hz using two CCD cameras with a resolution of 2448× 2048 (Grasshopper GRAS-50S5M, Teledyne FLIR LLC, Oregon, USA), and 35 mm focal length lenses (Point Grey Research, Richmond, BC, Canada). The system was calibrated using a standard calibration plate provided by Correlation Solutions and five images were captured before the insertion test to measure the static noise floor.

Images with the best image quality from the ten tests were selected for the DIC strain analysis. Regions of interest (ROI) ($y =$ 25~39 mm; and, $x =$ 2~38 mm, shown in Fig.1) were selected to analyze strains. Displacement field was calculated using image correlation software (VIC-3D, Correlated Solutions Inc, Irmo, South Carolina). In-plane Lagrange strain in the x-direction, ε_{x_DIC}, y-direction, ε_{y_DIC}, and *von Mises* strain, ε_{v_DIC}, were calculated from the resultant displacements:

$$\varepsilon_{x\_DIC} = \frac{du}{dx} + \frac{\left(\frac{du}{dx}\right)^2 + \left(\frac{dv}{dx}\right)^2}{2} \quad (1.1)$$

$$\varepsilon_{y\_DIC} = \frac{dv}{dy} + \frac{\left(\frac{du}{dy}\right)^2 + \left(\frac{dv}{dy}\right)^2}{2} \quad (1.2)$$

$$\varepsilon_{v\_DIC} = \frac{2}{3}\sqrt{\varepsilon_1^2 - \varepsilon_1\varepsilon_2 + \varepsilon_2^2} \quad (1.3)$$

where, u and v are displacements in the x and y directions in mm, respectively. ε_1 and ε_2 are the maximum principal and minimum principal strains, respectively.

2.2 Finite Element Analysis

The insertion process was simulated using a commercial FEA package: Abaqus Explicit version 2017 (Simulia, RI, USA). The insertion FE models were three-dimensional (3D); and, the analyses were dynamic, continuous and explicit. Details of model geometry and mesh, material properties, and boundary conditions are described as follows.

2.2.1 FEA Geometry and Mesh

Geometry of the FEA model was generated according to the experimental setup; and, the implant geometry was provided by the implant manufacturer. The implant and fixture were modelled as rigid bodies using 4-node 3D bilinear rigid quadrilateral elements (R3D4): 26,757 nodes for the CF implant, 8,936 for the NCF implant, and 200 for the bottom fixture. The PU foam block (40 × 40 × 8 mm) with a pilot hole (2.4/2.8 mm in diameter and 13 mm in length) was modelled using linear hexahedral elements with incompatible modes (C3D8I) and 757,800 nodes. Based on a mesh sensitivity study [24], to optimize solution accuracy and computational time, the mesh was refined near the osteotomy with 0.1 mm local edge length while the global edge length was 0.5 mm for the bone surrogate, shown in the Fig.2.

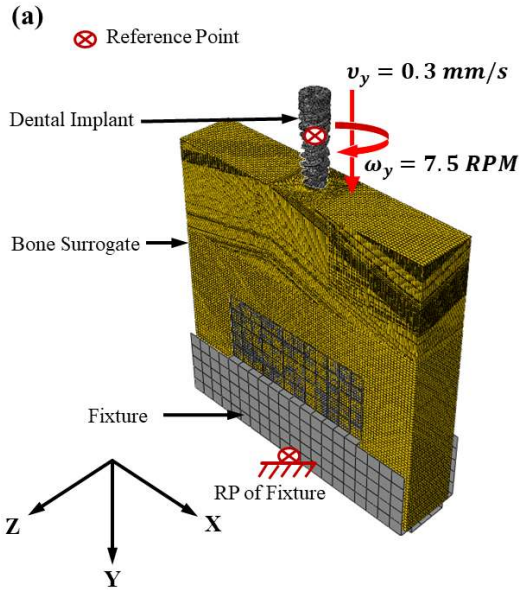

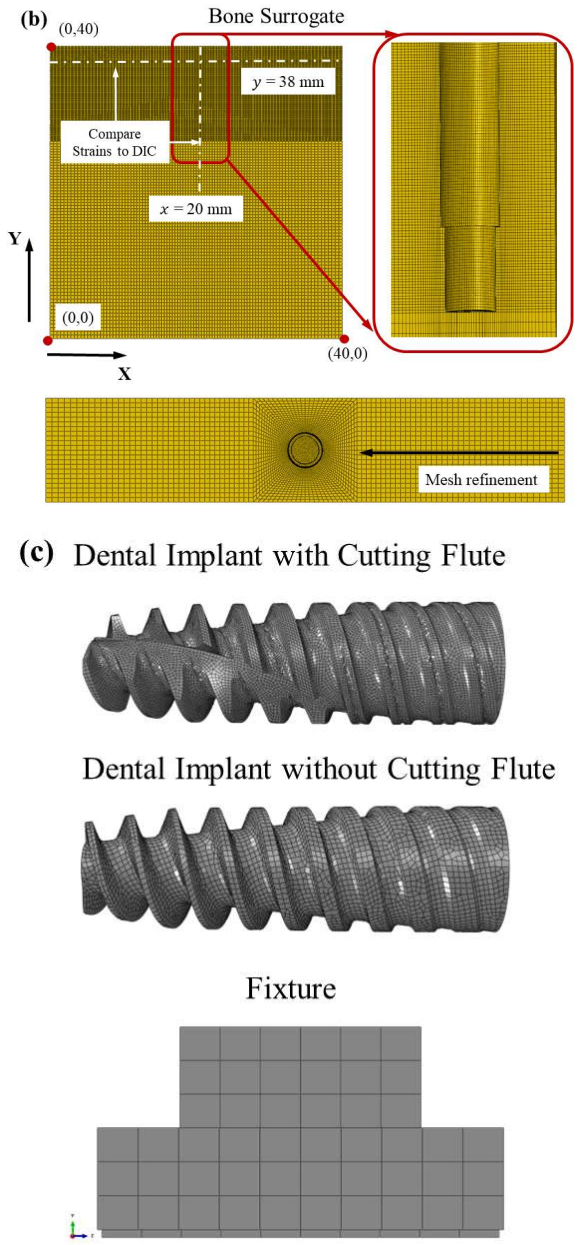

Figure 2: Details of FE model. (a) FEA geometry and boundary condition; (b) Mesh quality of bone surrogate, and coordinate. The *von Mises* strain (ε_v) location along y = 38 mm (horizontal line) or x = 20 mm (vertical line) were compared between the DIC measurements and FEA prediction. (c) Mesh quality of implants and fixture.

2.2.2 FEA Material Properties

The implant mass and rotational inertia were defined at the implant reference point (RP) located at the centre of mass while the RP for the fixture was located at the bottom in the center. The PU foam was modelled as a progressive crushable foam [25,26]. A series of quasi-static uniaxial compression tests with unloading-reloading cycles at 10, 20, 40, and 50% engineering strains, ε, were performed to measure the apparent elastic modulus, E, in MPa. The compression tests were conducted with a constant displacement rate of 0.08 mm/s and five repeats; and, the specimen size was 20 × 20 × 20 mm using Bionix tabletop test system Model 370.02 (MTS Systems Corporation, MN, USA). The apparent elastic modulus, E, at each loading cycles was calculated using the average value of loading and unloading slopes [27]:

$$E(\varepsilon) = \frac{E^L(\varepsilon)+E^U(\varepsilon)}{2} \quad (2)$$

where E^L and E^U were the elastic moduli of the loading and unloading paths in MPa, respectively.

The initial apparent elastic modulus, E_0, and yield strength were 123 MPa and 8.06 MPa, respectively. Table.1 lists the ratio of measured apparent elastic modulus to initial apparent modulus, E/E_0, at each engineering strain level. Linear elastic and multilinear plastic material models were used to approximately represent the PU foam. Damage evolution initiated at the onset of the plasticity plateau due to local buckling and micro damage [25,26]. A ductile damage model was used, considering the equivalent plastic strain, ε^{pl}, at the onset of damage as a function of stress triaxiality and strain rate, $\dot{\varepsilon}$, [28]:

$$\varepsilon^{pl}(\eta, \dot{\varepsilon}) \quad (3)$$

where η is the stress triaxiality. The damage was modelled as a degradation of the elasticity. The damage evolution was defined based on effective plastic displacement using an overall damage variable, D, [28]:

$$E = (1 - D)E_0 \quad (4)$$

when D reached 1, the material failed, and elements were deleted. The locked-up strain (the onset of the densification) was 0.3 which was estimated from the uniaxial compressive test. To confirm the PU foam material model could represent the foam mechanical behaviour under loading-unloading uniaxial compression, a numerical compression test was carried out in Abaqus, shown in Fig.3.

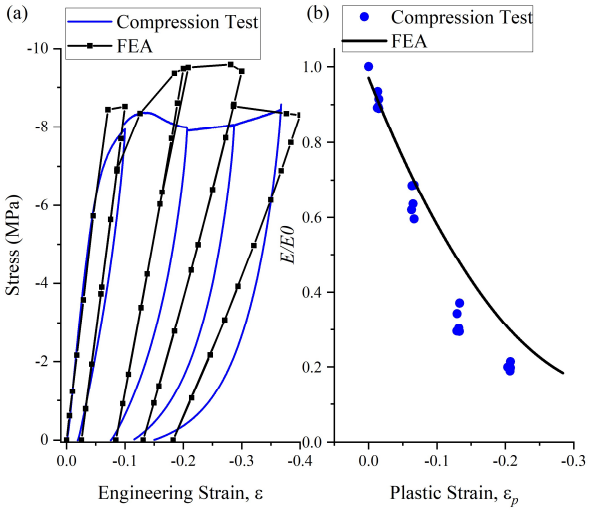

Figure 3: The FEA elastic-plastic material model (black) in comparison to the compression test (blue) of the PU foam. (a) Stress-engineering strain curves for the loading-unloading uniaxial compression test. (b) E/E_0 at four plastic strain levels.

Table 1 Average plastic strain, ε_p, ratio of the apparent elastic modulus to the initial elastic modulus, E/E_0, and the overall damage variable, D at each engineering strain level.

Engineering Strain	0	10%	20%	30%	40%	50%
Plastic Strain, ε_p	0	0.0020	0.050	0.11	0.16	0.22
E/E_0	1.0	1.0	0.73	0.46	0.26	0.19
D	0	0	0.27	0.54	0.74	0.81

2.2.3 FEA Boundary Conditions

The fixture RP was fixed in all six degrees of freedom while the implant was only allowed to rotate around and move in the y-direction (axial) with constant angular velocity of 7.5 rpm and axial velocity of 0.3 mm/s, shown in Fig.2a.

General contact algorithm of Abaqus [28] was used with element-based surfaces between the PU foam and implant and applied to new exposed element-surfaces after element deletion. A penalty formulation was adopted for friction tangential behaviour between the foam and implant with a constant coefficient of 0.61 [22,29]. Rough formulation (no slip) was used between the foam and the fixture.

2.3 FEA Validation Procedure

Comparison between DIC measurements and FE predictions was focused on in-plane Lagrange *von Mises* strain, ε_v, because the ε_v is an invariant of strain tensor independent of the coordinate system. The FEA in-plane Lagrange *von Mises* strain, ε_{v_FEA}, was calculated using the same equation 1.3 as DIC measurements. Distribution of in-plane Lagrange *von Mises* strain measured on the front surface of the PU foam with DIC, ε_{v_DIC}, was compared to the FEA results, ε_{v_FEA}, at insertion depths of 3, 5.4, 7.8, 10.2, 11.5 mm. The ε_v location along y = 38 mm (horizontal line) or x = 20 mm (vertical line) were compared between the DIC measurements and FEA prediction at the five insertion depths (white dashed lines in Fig.2b). In addition, a linear regression between the DIC measurements and FEA predictions was carried out for the ε_v along the horizontal line (y = 38mm) at the final insertion depth to evaluate the overall FEA performance using IBM SPSS Statistics 25 (IBM Corporation, Armonk, New York, USA).

3. RESULTS AND DISCUSSION

The in-plane Lagrange *von Mises* strain, ε_v, on the PU foam surface was compared between the DIC measurement and FEA prediction to validate the strain analysis for this study. Uncertainty of DIC measurement in both X and Y displacements was 0.6 μm; and the static noise floor for the strain measurement was 500 microstrain ($\mu\varepsilon$). Distribution of ε_v on the PU foam surface was comparable between DIC measurements and FEA prediction at the five insertion depths (Fig.4 and 5). For the maximum in-plane Lagrange *von Mises* strain, ε_{v_max}, over the entire ROI at the final insertion depth (11.5mm), the FEA prediction for the CF and NCF implants was 2.7% lower and 8.3 % higher than the DIC, respectively. The coefficient of determination (R^2) for ε_v between DIC and FEA along the horizontal line for the CF and NCF implants were 0.80 and 0.78 (slopes of 0.86 and 0.78), respectively (Fig.5). The insertion torques, IT, predicted by FEA were substantially lower than the measurements in the mechanical test (Fig.6a). The deformed shapes near the osteotomy predicted by FEA were similar to the mechanical test (Fig.6b).

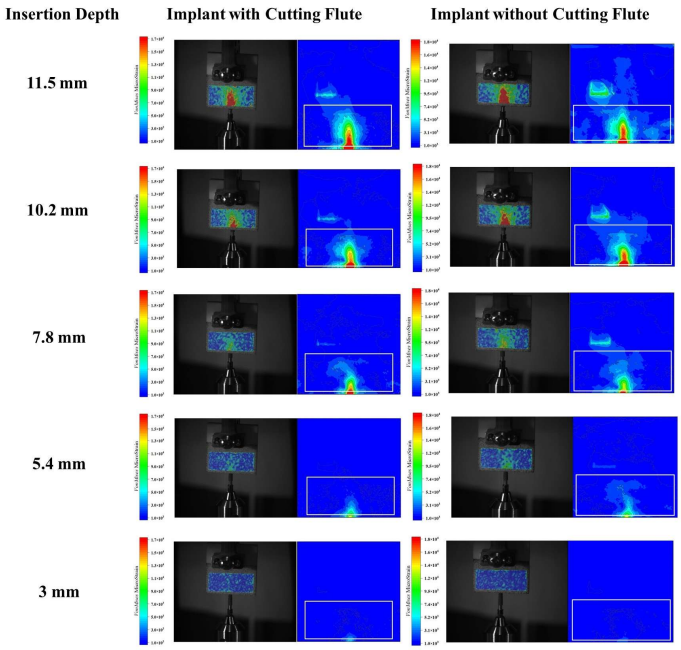

Figure 4: Distributions of von Mises strain, ε_v, were comparable between DIC measurements and FEA predictions at the insertion depths of 3, 5.4, 7.8, 10.2, 11.5 mm.

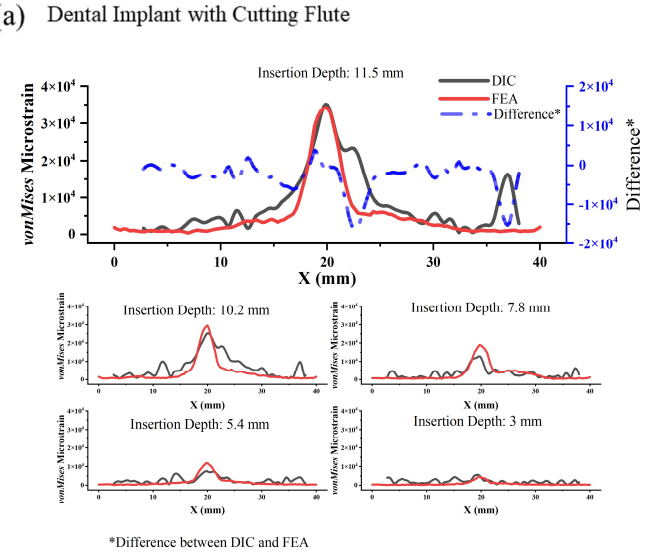

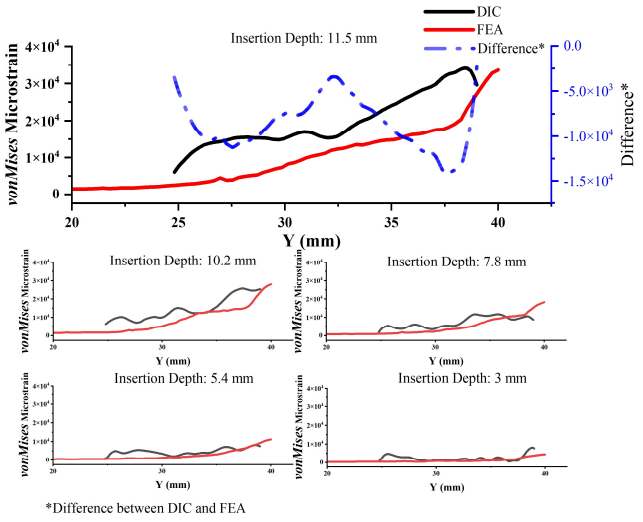

(b) Dental Implant without Cutting Flute

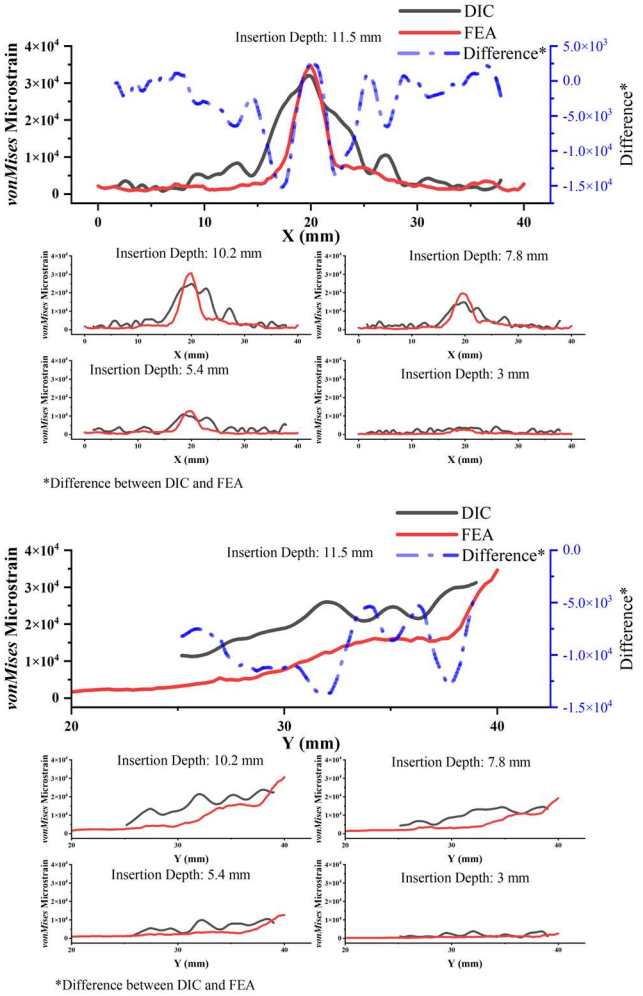

Figure 5: The *von Mises* strain, ε_v, calculated from FEA were lower than DIC measurements along the horizontal and vertical lines. The ε_v along the horizontal (right) and vertical (left) lines for the implant with cutting flute (a) and without cutting flute (b) at different insertion depths, respectively.

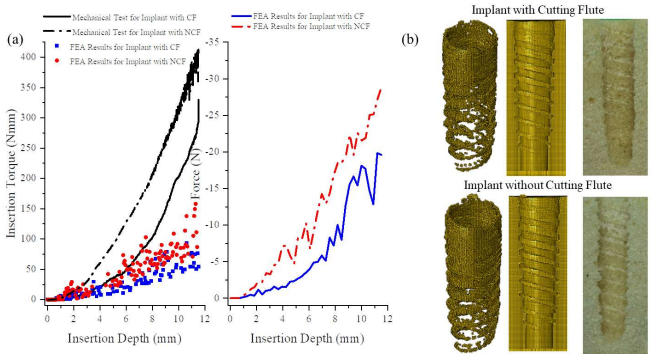

Figure 6: A lower axial force (<20N for the implant with cutting flute (CF)) suggested that thread forming dominated during the insertion instead of extrusion at higher loads (a) The insertion torques predicted by FEA were substantially lower than the measurements of the mechanical test. The IT for the CF implant black solid line; implant without cutting flute (NCF) black dash-dot line; the CF implant predicted by FEA blue square dots and the NCF implant predicted by FEA red dots. The axial force predicted by FEA for the CF implant (blue solid line) and NCF implant (red dash-dot line). (b) Shape of deformed osteotomy predicted by FEA was comparable to the experimental test. Top: an isometric view of the undeformed deleted elements (left), a section view of the deformed osteotomy predicted by FEA (middle) and observed in mechanical test (right) for the CF implant; Bottom: for the NCF implant.

The area with surface ε_{v_DIC} above 5000 $\mu\varepsilon$ was wider for the NCF implant than CF implant at the final insertion depth (Fig.4). A similar result was observed from the FEA prediction (Fig.7). The IT and insertion axial force for the NCF implant were higher than the CF implant while the damage volume (volume of the element with D > 0) in the bone for the NCF implant (27.5 mm^3) was 17 % higher than the CF implant under the evaluated conditions. Likewise, the volume with maximum shear stress larger than 1 MPa for the CF implant was smaller than the NCF implant (Fig.8).

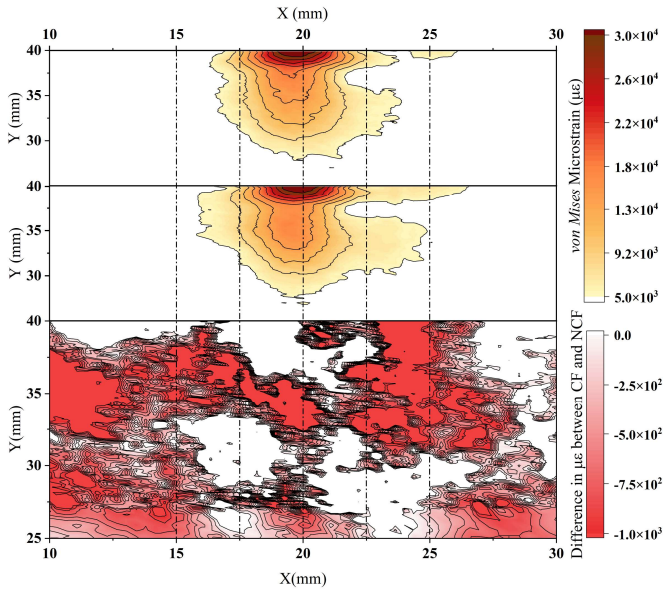

Figure 7: From the FEA prediction, the surface *von Mises* strain, ε_{v_FEA}, above 5000 $\mu\varepsilon$ for implant without cutting flute (NCF) was wider than the implant with cutting flute (CF) at the final insertion depth: the surface ε_{v_FEA} distribution for the CF implant (top), surface ε_v distribution for the NCF implant (middle), and the difference between the CF and NCF implant.

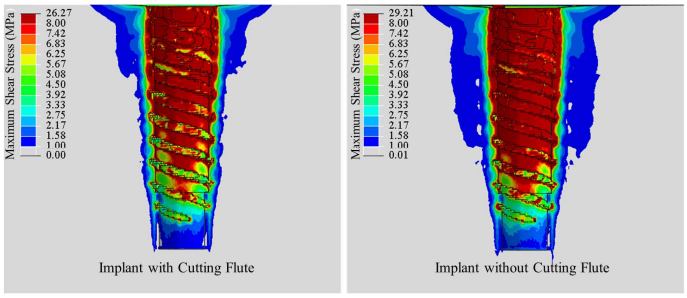

Figure 8: The Maximum shear stress in the PU foam: left is for the implant with cutting flute; and, right is for the implant without cutting flute.

The combination of experimental measurements and computer simulations provides a reliable and comprehensive method to study the mechanics of dental implant insertion. The purpose of this study was to: 1. compare the difference between DIC strain measurements with FEA predictions; and, 2. to investigate the effect of a cutting flute during dental implant insertion.

The DIC technique offers the advantage of a precise full-field strain measurement; however, several factors affect measurement accuracy [30]. The DIC data uncertainty is highly dependent on the system setup such as lighting, quality of the speckle pattern, and camera lens distortion [7,31]. Appropriate calibration and validation processes of the DIC system are required to obtain accurate measurements. However, there is no standard calibration or validation process for DIC [7]. Studies have shown that with a good setup the uncertainty of DIC system could be reduced to 5 μm (5%) for the order of 100 μm displacements [32,33]. Moreover, others used FEA and other optical techniques such as photoelasticity to validate DIC measurements [34-36]. In this study, the uncertainty in displacement measurements was 6 μm (2.5%) which suggested the DIC setup was appropriate. Agreement between the FEA predictions and the DIC further supported the reliability of the DIC measurements.

The ε_{v_FEA} on the bone surrogate surface was comparable to DIC measurements and in accordance with the literature [21,22]. Utility of FEA in biomechanics has been the subject of criticism due to inadequate verification and validation [16]. In this study, at the material level, the PU foam mechanical behaviour was measured with uniaxial compression tests and predicted using FEA, with good agreement (Fig.3). At the complete system level, since the strain is the parameter of interest, this study validated the FEA directly by comparing ε_v on the PU foam surface to experimental DIC measurements. The regression analysis of the FEA versus DIC demonstrated a strong correlation indicating good model agreement overall (R^2=0.80 and 0.78 for the CN and NCF implants, respectively).

The IT predicted by the FEA was lower than the measured IT, similar to findings in other studies [21,22]. In Dorogoy's FEA study, the maximum IT was around 200 Nmm with a material yield strength of 10 MPa and the vertical force was under 20 N [22]. In their FEA, Ovesy et al. predicted a maximum IT around 150 Nmm in low density bovine trabecular bone for the same implant analysed as the current study [21]. The current FEA underestimated the IT with similar explanations for the low prediction to the Ovesy's discussion: in the numerical model, elements were deleted when strain exceeded the failure criterion; however, the PU foam chips remained in the osteotomy during the insertion test which continued to contribute the IT. The element deletion also caused a "numerical' vibration in the IT (Fig.6), which was also observed in both Dorogoy's and Ovesy's FEA studies [21,22].

Another interesting observation was non-zero axial reaction forces. Dorogoy's FEA defined a series of constant axial forces on the implant to initiate the insertion procedure. Due to the IT and axial force, both thread and extrusion forming phenomena existed during the insertion. When the axial force was less than 20 N, the insertion was dominated by thread forming rather than extrusion as demonstrated by the easily distinguished threads in the osteotomy [22]. In the current FEA study, a constant axial speed was defined, and the FEA predicted an axial force less than 20 N for the CF implant during the insertion; and, threads in the osteotomy were easily distinguished after the insertion (Fig.6). Together, the results suggested the thread forming phenomenon dominated the insertion process for the CF implant; and, similar mechanics for the NCF implant.

Previous work by the authors [23,37] found, and the DIC and FEA results of the current study confirmed, the cutting flute facilitated insertion. The lower IT for the CF implant was observed compared to the NCF implant both in the FEA and the mechanical test. An analytical model proposed by Yang et al.

offers an explanation for the mechanics of the cutting flute which decreased the force and increased the pressure [23]. The same observation was found in the current computational study: the maximum shear stress in the PU foam and axial force were lower for the CF implant in comparison to NCF implant (Fig.8). During the insertion, the applied torque forms threads in the PU foam [37]. The cutting flute facilitated the insertion, which resulted in less effort (lower IT and axial force) to form the thread. In addition, the IT not only forms the thread but also generates deformation in the PU foam (Fig.7) and is therefore associated with increased maximum shear stress (Fig.8).

There are several limitations in this study. Firstly, the implant insertion was performed on PU foam under lab conditions instead of human bone in clinical environments. However, preclinical experimental data is vital in support of the design of subsequent cadaveric, *in vivo* animal and clinical trials [38]. In particular, preclinical experiments allow researchers to perform uni- and multivariate experiments [39] and the PU foam used as a bone surrogate has been approved as a standard material for preclinical testing of orthopedic devices by the American Society for Testing and Materials (ASTM F1839-08). Secondly, the IT was underestimated in the FEA, which may be due to inaccurate modelling of densification in the material modelling. If accurate IT is required for the intended of use, further studies are required to improve the FEA performance for IT prediction. In addition, further sensitivity studies on FEA model parameters are required to improve model credibility including verification, uncertainty quantification, and risks relating to context of use. However, the overall FEA performance on the surface ε_v had a good agreement with the experimental DIC results (R^2=0.80 and 0.78 for the CN and NCF implants, respectively). In addition, the FEA results indicated the cutting flute reduced the maximum shear stress in the PU foam and axial force, which facilitated the insertion with less effort. FEA of the insertion process demonstrated non-negligible stress and strain in the bone surrogate contributing to the biomechanics of the dental implant.

4. CONCLUSION

This study demonstrated the successful combination of mechanical testing and FEA to better understand the mechanics of dental implant insertion.

ACKNOWLEDGEMENTS

We acknowledge funding from Nobel Biocare Services AG (Biomechanics-R17004/P17047 & R19003), the support of the Natural Sciences and Engineering Research Council of Canada/le Conseil de recherches en sciences naturelles et en génie du Canada (NSERC/CRSNG), Canadian Foundation Innovation/Fondation Canadienne pour l'Innovation John R. Evans Leaders Fund (CFI/FCI JELF), Ploeg's Research Initiation Grant, and the Centre for Health Innovation, Queen's University, Kingston, ON, Canada. Amal Saade and Maria Teresa, Barletta contribution to the editing of this text is gratefully acknowledged.

REFERENCES

[1] Mangano, F., Leandro Chambrone, R. Van Noort, C. Miller, P. Hatton, and C. Mangano. "Direct metal laser sintering titanium dental implants: a review of the current literature." *International journal of biomaterials* 2014 (2014). DOI: 10.1155/2014/461534

[2] Javed, Fawad, Hameeda Bashir Ahmed, Roberto Crespi, and Georgios E. Romanos. "Role of primary stability for successful osseointegration of dental implants: Factors of influence and evaluation." *Interventional Medicine and Applied Science* 5, no. 4 (2013): 162-167. DOI: 10.1556/IMAS.5.2013.4.3

[3] Khan, Akhtar S., and Xinwei Wang. *Strain measurements and stress analysis*. 2001.

[4] Grassi, Lorenzo, and Hanna Isaksson. "Extracting accurate strain measurements in bone mechanics: A critical review of current methods." *Journal of the mechanical behavior of biomedical materials* 50 (2015): 43-54. DOI: 10.1016/j.jmbbm.2015.06.006

[5] Li, Jian-ying, Andrew Lau, and Alex SL Fok. "Application of digital image correlation to full-field measurement of shrinkage strain of dental composites." *Journal of Zhejiang University SCIENCE A* 14, no. 1 (2013): 1-10. DOI: https://doi.org/10.1631/jzus.A1200274

[6] Palanca, Marco, Gianluca Tozzi, and Luca Cristofolini. "The use of digital image correlation in the biomechanical area: a review." *International biomechanics* 3, no. 1 (2016): 1-21. DOI: http://dx.doi.org/10.1080/23335432.2015.1117395

[7] Yoon, Sungsik, Hyung-Jo Jung, J. C. Knowles, and Hae-Hyoung Lee. "Digital image correlation in dental materials and related research: A review." *Dental Materials* 37, no. 5 (2021): 758-771.

[8] Chuang, Shu-Fen, T. Y. Chen, and Chih-Han Chang. "Application of digital image correlation method to study dental composite shrinkage." *Strain* 44, no. 3 (2008): 231-238. DOI: https://doi.org/10.1007/978-981-10-4361-1_11

[9] Tiossi, Rodrigo, Lianshan Lin, Renata CS Rodrigues, Young C. Heo, Heather J. Conrad, C. Maria da Gloria, Ricardo F. Ribeiro, and Alex SL Fok. "Digital image correlation analysis of the load transfer by implant-supported restorations." *Journal of biomechanics* 44, no. 6 (2011): 1008-1013. DOI: 10.1016/j.jbiomech.2011.02.015

[10] Tiossi, Rodrigo, Lianshan Lin, Heather Joan Conrad, Renata CS Rodrigues, Young Cheul Heo, Maria da Gloria Chiarello de Mattos, Alex Sui-Lun Fok, and Ricardo Faria Ribeiro. "A digital image correlation analysis on the influence of crown material in implant-supported prostheses on bone strain distribution." *Journal of prosthodontic research* 56, no. 1 (2012): 25-31. DOI: 10.1016/j.jpor.2011.05.003

[11] Tiossi, Rodrigo, Marco AA Vasco, Lianshan Lin, Heather J. Conrad, Osvaldo L. Bezzon, Ricardo F. Ribeiro, and Alex SL Fok. "Validation of finite element models for strain analysis of implant-supported prostheses using digital image correlation." *Dental Materials* 29, no. 7 (2013): 788-796. DOI: https://doi.org/10.1016/j.dental.2013.04.010

[12] Clelland, Nancy L., Burak Yilmaz, and Jeremy D. Seidt. "Three-Dimensional Image Correlation Analyses for Strains

Generated by Cement and Screw-Retained Implant Prostheses." *Clinical implant dentistry and related research* 15, no. 2 (2013): 271-282. DOI: 10.1111/j.1708-8208.2011.00411.x
[13] Salaita, Louai G., Burak Yilmaz, Jeremy D. Seidt, Nancy L. Clelland, Hua-Hong Chien, and Edwin A. McGlumphy. "Strain analysis of 9 different abutments for cement-retained crowns on an internal hexagonal implant." *The Journal of Prosthetic Dentistry* 118, no. 2 (2017): 166-171. DOI: 10.1016/j.prosdent.2016.10.008
[14] de Carvalho, Eduardo Bortolas, Paulo Eduardo Herbst, Adriana Cláudia Lapria Faria, Ricardo Faria Ribeiro, Priscila Paganini Costa, and Rodrigo Tiossi. "Strain transfer behavior of different planning options for mandibular single-molar replacement." *The Journal of Prosthetic Dentistry* 119, no. 2 (2018): 250-256. DOI: 10.1016/j.prosdent.2017.03.017
[15] Chang, Yuanhan, Abhijit Anil Tambe, Yoshinobu Maeda, Masahiro Wada, and Tomoya Gonda. "Finite element analysis of dental implants with validation: to what extent can we expect the model to predict biological phenomena? A literature review and proposal for classification of a validation process." *International journal of implant dentistry* 4, no. 1 (2018): 1-14. DOI: 10.1186/s40729-018-0119-5
[16] Anderson, Andrew E., Benjamin J. Ellis, and Jeffrey A. Weiss. "Verification, validation and sensitivity studies in computational biomechanics." *Computer methods in biomechanics and biomedical engineering* 10, no. 3 (2007): 171-184.
[17] Schwer, Leonard E. "Verification and validation in computational solid mechanics and the ASME Standards Committee." *WIT Transactions on the Built Environment* 84 (2005).
[18] American Society of Mechanical Engineers. "Guide for verification and validation in computational solid mechanics." ASME, 2006.
[19] Van Staden, Rudi C., Hong Guan, Newell W. Johnson, Yew-Chaye Loo, and Neil Meredith. "Step-wise analysis of the dental implant insertion process using the finite element technique." *Clinical oral implants research* 19, no. 3 (2008): 303-313. DOI; https://doi.org/10.1111/j.1600-0501.2007.01427.x
[20] Guan, Hong, Rudi C. Van Staden, Newell W. Johnson, and Yew-Chaye Loo. "Dynamic modelling and simulation of dental implant insertion process—A finite element study." *Finite Elements in Analysis and Design* 47, no. 8 (2011): 886-897. DOI: 10.1016/j.finel.2011.03.005
[21] Ovesy, Marzieh, Michael Indermaur, and Philippe K. Zysset. "Prediction of insertion torque and stiffness of a dental implant in bovine trabecular bone using explicit micro-finite element analysis." *Journal of the mechanical behavior of biomedical materials* 98 (2019): 301-310. DOI: https://doi.org/10.1016/j.jmbbm.2019.06.024
[22] Dorogoy, A., D. Rittel, K. Shemtov-Yona, and R. Korabi. "Modeling dental implant insertion." *Journal of the mechanical behavior of biomedical materials* 68 (2017): 42-50. DOI: https://doi.org/10.1016/j.jmbbm.2017.01.021
[23] Yang, Baixuan, Ainara Irastorza-Landa, Peter Heuberger, and Heidi-Lynn Ploeg. "Analytical model for dental implant insertion torque." *Journal of the Mechanical Behavior of Biomedical Materials* 131 (2022): 105223. DOI: https://doi.org/10.1016/j.jmbbm.2022.105223
[24] Yang, Baixuan, 2018, "Dental Implant Insertion, A Mechanical Investigation with Experiments and Simulations," M.S. dissertation, University of Wisconsin-Madison, Madison, WI.
[25] Flores-Johnson, E. A., Q. M. Li, and R. A. W. Mines. "Degradation of elastic modulus of progressively crushable foams in uniaxial compression." *Journal of cellular plastics* 44, no. 5 (2008): 415-434. DOI: https://doi.org/10.1177/0021955X08095113
[26] Li, Q. M., and R. A. W. Mines. "Strain measures for rigid crushable foam in uniaxial compression." *Strain* 38, no. 4 (2002): 132-140. DOI: https://doi.org/10.1111/j.1475-1305.2002.00029.x
[27] Sugimura, Y., J. Meyer, M. Y. He, H. Bart-Smith, J. Grenstedt, and A. G. Evans. "On the mechanical performance of closed cell Al alloy foams." *Acta materialia* 45, no. 12 (1997): 5245-5259. DOI: https://doi.org/10.1016/S1359-6454(97)00148-1
[28] Abaqus, G. "Abaqus 6.11." *Dassault Systemes Simulia Corporation, Providence, RI, USA* (2011).
[29] Grant, J. A., N. E. Bishop, N. Götzen, C. Sprecher, M. Honl, and M. M. Morlock. "Artificial composite bone as a model of human trabecular bone: the implant–bone interface." *Journal of biomechanics* 40, no. 5 (2007): 1158-1164. DOI: 10.1016/j.jbiomech.2014.01.029
[30] Jones, E. M., and M. A. Iadicola. "International Digital Image Correlation Society." *A Good Practices Guide for Digital Image Correlation* 10 (2018).
[31] Pan, Bing, Kemao Qian, Huimin Xie, and Anand Asundi. "Two-dimensional digital image correlation for in-plane displacement and strain measurement: a review." *Measurement science and technology* 20, no. 6 (2009): 062001. DOI: 10.1088/0957-0233/20/6/062001
[32] Sebastian, C., and E. A. Patterson. "Calibration of a digital image correlation system." *Experimental Techniques* 39, no. 1 (2015): 21-29. DOI: https://doi.org/10.1111/ext.12005
[33] Chuang, Shu-Fen, Chih-Han Chang, and Terry Yuan-Fang Chen. "Spatially resolved assessments of composite shrinkage in MOD restorations using a digital-image-correlation technique." *Dental materials* 27, no. 2 (2011): 134-143. DOI: 10.1016/j.dental.2010.09.008
[34] Tiossi, Rodrigo, Erica M. De Torres, Renata CS Rodrigues, Heather J. Conrad, C. Maria da Gloria, Alex SL Fok, and Ricardo F. Ribeiro. "Comparison of the correlation of photoelasticity and digital imaging to characterize the load transfer of implant-supported restorations." *The Journal of Prosthetic Dentistry* 112, no. 2 (2014): 276-284. DOI: 10.1016/j.prosdent.2013.09.029
[35] Wang, Yueqi, Pascal Lava, Sam Coppieters, Maarten De Strycker, Paul Van Houtte, and Dimitri Debruyne. "Investigation of the uncertainty of DIC under heterogeneous strain states with numerical tests." *Strain* 48, no. 6 (2012): 453-462.

[36] Cantó-Navés, Oriol, Xavier Marimon, Miquel Ferrer, and Josep Cabratosa-Termes. "Comparison between experimental digital image processing and numerical methods for stress analysis in dental implants with different restorative materials." *Journal of the mechanical behavior of biomedical materials* 113 (2021): 104092. DOI: 10.1016/j.jmbbm.2020.104092

[37] Yang, Baixuan, Ainara Irastorza-Landa, Peter Heuberger, and Heidi-Lynn Ploeg. "Effect of insertion factors on dental implant insertion torque/energy-experimental results." *Journal of the Mechanical Behavior of Biomedical Materials* 112 (2020): 103995. DOI: 10.1016/j.jmbbm.2020.103995

[38] Faggion Jr, Clovis Mariano. "Guidelines for reporting pre-clinical in vitro studies on dental materials." *Journal of Evidence Based Dental Practice* 12, no. 4 (2012): 182-189. DOI: 10.1016/j.jebdp.2012.10.001

[39] White, D. J. "The application of in vitro models to research on demineralization and remineralization of the teeth." *Advances in dental research* 9, no. 3 (1995): 175-193. DOI: https://doi.org/10.1177/08959374950090030101